Stopping Power of Swift Hydrogen and Helium Ions in Gases

By F. BESENBACHER, H. H. ANDERSEN,
P. HVELPLUND, *and* H. KNUDSEN

Det Kongelige Danske Videnskabernes Selskab
Matematisk-fysiske Meddelelser **40**:3

Kommissionær: Munksgaard
1979

DET KONGELIGE DANSKE VIDENSKABERNES SELSKAB
udgiver følgende publikationsrækker:

THE ROYAL DANISH ACADEMY OF SCIENCES AND LETTERS
issues the following series of publications:

	Bibliographical Abbreviation
Oversigt over Selskabets Virksomhed (8°) *(Annual in Danish)*	Overs. Dan. Vid. Selsk.
Historisk-filosofiske Meddelelser (8°)	Hist. Filos. Medd. Dan. Vid. Selsk.
Historisk-filosofiske Skrifter (4°) *(History, Philology, Philosophy, Archaeology, Art History)*	Hist. Filos. Skr. Dan. Vid. Selsk.
Matematisk-fysiske Meddelelser (8°) *(Mathematics, Physics, Chemistry, Astronomy, Geology)*	Mat. Fys. Medd. Dan. Vid. Selsk.
Biologiske Skrifter (4°) *(Botany, Zoology, General Biology)*	Biol. Skr. Dan. Vid. Selsk.

Selskabets sekretariat og postadresse
The address of the Academy is:

Det Kongelige Danske Videnselskabernes Selskab,
Dantes Plads 5,
DK-1556 Copenhagen V.
Denmark.

Selskabets kommissionær
The publications are sold by the agent of the Academy:

MUNKSGAARDS BOGHANDEL,
6, Nørregade,
DK-1165 Copenhagen K.
Denmark.

Stopping Power of Swift Hydrogen and Helium Ions in Gases

By F. BESENBACHER, H. H. ANDERSEN,
P. HVELPLUND, *and* H. KNUDSEN

Det Kongelige Danske Videnskabernes Selskab
Matematisk-fysiske Meddelelser **40**: 3

Kommissionær: Munksgaard
1979

Contents

Synopsis

Stopping powers of H_2, He, N_2, O_2, CO_2, Ne, Ar, Kr, and Xe for 40-keV to 1-MeV hydrogen ions and 100-keV to 2.4-MeV helium ions have been measured to an accuracy of $\pm 2.5\%$ (2σ). The stopping powers for hydrogen show good agreement with most other published results and with the Andersen and Ziegler tabulations, while those for helium ions are up to 6% lower than the helium data of Chu and Powers. With higher-order Z_1 correction terms included in the theoretical description, Bonderup's calculated shell-corrections based on the Lindhard-Scharff model, are in good agreement with the experimental proton data for $E_p \geq 100$ keV, and experimental I values may be deduced. Within the velocity region $4.4 \lesssim v/v_0 \lesssim 4.9$ and for target materials with $1 \leq Z_2 \leq 54$, the experimental findings support Lindhard's and Esbensen's value for the Barkas correction. The stopping-power ratios S_{He}/S_H depend strongly on Z_2 and deviate significantly from the mean-square charge state obtained from experimental equilibrium charge state distributions.

Institute of Physics, University of Aarhus
DK-8000 Aarhus C, Denmark

Printed in Denmark by Bianco Lunos Bogtrykkeri A/S. ISSN 0023-3323. ISBN 87-7304-097-5

§1. Introduction

The energy loss of an ion beam traversing matter is a phenomenon of basic interest to atomic physics and has been the subject of much theoretical and experimental work. However, there is still a great need for a better understanding of the details of the stopping processes.

It is the purpose of the present work, through accurate measurements to test the Lindhard-Scharff model (Lindhard and Scharff 1953, 1960) and its refinements for the average energy-loss (Bonderup 1967) and energy straggling (Bonderup and Hvelplund 1971). Especially it is of interest to examine the so-called shell corrections at the present rather low energies, and to investigate Sigmund's molecular correlation effect in energy straggling (Sigmund 1976).

A detailed understanding of the underlying mechanisms is imperative for obtaining the kind of comprehensive and accurate energy loss and straggling information necessary in, for example, a composition analysis of thin films via Rutherford-backscattering or nuclear reaction techniques.

We have carried out a systematic investigation of the stopping power and energy straggling for hydrogen and helium ions in H_2, He, N_2, O_2, CO_2, Ne, Ar, Kr, and Xe at ion energies 40 keV $\lesssim E_H \lesssim$ 1 MeV and 100 keV $\lesssim E_{He} \lesssim$ 2.4 MeV. Gaseous targets were chosen so as to avoid specific solid-state effects that might obscure especially the straggling results.

The present paper deals with the stopping-power results only. A forthcoming publication (Besenbacher et al. 1980) will deal with the straggling results, some of which have already been published (Besenbacher et al. 1977).

After a brief review of the energy-loss theory in §2, the experimental procedure and data treatment will be discussed in §3. In §4, the experimental results will be presented and compared with empirical stopping-power tabulations and other published results and, finally, in §5, the experimental data will be discussed and compared with theory.

§2. Theory

As discussed by Bohr (1948), two distinctly different mechanisms are responsible for the slowing-down of nonrelativistic charged particles: (*i*) Electronic stopping, i.e., energy loss to excitation and ionization, and (*ii*) Nuclear stopping, i.e., energy transfer leading to translatory motion of the struck atom as a whole. In the present velocity range $v \gtrsim v_o$ (v_o is the Bohr velocity $e^2/\hbar$), and with our experimental geometrical arrangement, the nuclear energy loss is almost negligible (see below).

At high velocities, where

$$\varkappa_B = \frac{2\mathcal{Z}_1 v_o}{v} < 1\,, \tag{1}$$

a quantal perturbation treatment is applicable and gives the wellknown Bethe formula (Bethe 1930). According to this formula, the specific electronic energy loss suffered by a heavy incoming particle with charge $\mathcal{Z}_1 e$ and velocity v penetrating a target of atomic number $\mathcal{Z}_2$ and density N (atoms per unit volume) is given by

$$\left(-\frac{dE}{dR}\right)_e = \frac{4\pi \mathcal{Z}_1^2 e^4}{mv^2} N \mathcal{Z}_2 L(v, \mathcal{Z}_2) \tag{2}$$

where

$$L(v, \mathcal{Z}_2) = L_o = \log\left(\frac{2mv^2}{I}\right) - \log\left(1 - \left(\frac{v}{c}\right)^2\right) - \left(\frac{v}{c}\right)^2 - \frac{C(v, \mathcal{Z}_2)}{\mathcal{Z}_2} \tag{3}$$

Here, m and $-e$ are the electron mass and charge, respectively, and c the velocity of light. The main parameters of the Bethe formula are the mean ionization potential I and the shell corrections $C/\mathcal{Z}_2$. The former is defined by

$$\log I = \frac{1}{\mathcal{Z}_2} \sum_i f_{oi} \log \hbar\, \omega_{oi} \tag{4}$$

where f_{oi} are the dipole oscillator strengths corresponding to the transition frequencies ω_{oi} for the atomic system. A direct calculation of I from this formula has until recently been impeded due to the lack of knowledge about the distribution of oscillator strength in the relevant energy region, i.e., from 10-1000 eV. In a Thomas-Fermi model the calculation of I is very much simplified since f_{oi} is a function of $\omega/\mathcal{Z}_2$ only and Bloch (1933) showed within this model that

$$I/\mathcal{Z}_2 = I_o = \text{constant}. \tag{5}$$

This result is in qualitative agreement with the experimental results for heavier atoms and empirically I_o is of the order of 10 eV. For lighter atoms the cut-off in $f(\omega, \mathcal{Z}_2)$ close to the Rydberg frequency leads to a somewhat higher value of $I/\mathcal{Z}_2$ (Lindhard 1964).

To calculate $L(v, \mathcal{Z}_2)$ in formula (2) and thereby to determine the mean ionization potential and the shell corrections, Lindhard and Scharff (1953, 1960) considered the target as a collection of free electron gases. The function $L(v, \mathcal{Z}_2)$ pertaining to an atom was obtained as an average over the electron

cloud of the quantity $L(\varrho, v)$ for a gas of density ϱ (Lindhard 1954). As a first approximation, they introduced the expression

$$L(v, Z_2) = \frac{1}{Z_2} \int 4\pi r^2 \varrho(r) \cdot L(r, v) dr$$

$$= \frac{1}{Z_2} \int_{r_{min}}^{\infty} 4\pi r^2 \varrho(r) \cdot \log \frac{2mv^2}{\gamma \hbar \omega_o(r)} dr \; ; \; \frac{2mv^2}{\gamma \hbar \omega_o(r_{min})} = 1 \qquad (6)$$

Here $\varrho(r)$ is the electron density of the target atom, $\omega_o(r)$ is the local plasma frequency $(4\pi e^2 \varrho(r)/m)^{1/2}$; and γ is a constant of the order of $\sqrt{2}$ by means of which they took into account the binding of the electrons. In the Lindhard-Scharff model the mean ionization potential can be calculated from

$$\log I = \frac{1}{Z_2} \int 4\pi r^2 \varrho(r) \log [\gamma \hbar \omega_o(r)] \, dr \qquad (7)$$

Bonderup and Lindhard (1967) and Chu and Powers (1972) calculated I from this formula using Hartree-Fock charge distributions and found significant oscillations superimposed on a slow decrease of I/Z_2 with increasing Z_2. Even though formula (7) was based on qualitative arguments, the results of the calculations agree fairly well with experiments. It deserves attention that very recently Inokuti et al. (1978) calculated I values by directly using formula (4) in a form appropriate for a continuous distribution of oscillator strengths. They started with the Hartree-Slater central potential model and carried through explicit calculations of df/dE for the entire spectrum from the dipole matrix elements between initial and final electron states. The variation of their I/Z_2 values with Z_2 is similar to that based on the Lindhard-Scharff model which, however, generally gives approximately 30% higher results. This ratio is close to the number $\gamma \sim \sqrt{2}$ which appears as a factor in the I value obtained from formula (7). This result lends strong support to formula (7).

The results based on the Lindhard-Scharff model were so promising even down to velocities of the order of a few times v_o that it was natural to repeat the averaging procedure in formula (6) with a more accurate expression for the electron gas function $L(\varrho, v)$. This was done by Lindhard and Winther (1964), and Bonderup (1967) applied their electron gas results to compute the shell corrections C/Z_2 in formula (3). The first-order Lenz-Jensen distribution was used for the function $\varrho(r)$. The function C/Z_2 is useful in a comparison between theory and experiment since, in contrast to the I value, this quantity is rather insensitive to the details in the distribution of the outermost electrons.

Since the Bethe treatment is based on a first-order perturbation calculation,

the resulting stopping power is proportional to $\mathcal{Z}_1^2$. However, both range measurements by Barkas (for a survey, see Heckman 1970) and accurate p and α stopping power measurements by Andersen et al. (1969) provided convincing evidence for the existence of higher-order $\mathcal{Z}_1$ correction terms to the stopping formula. Expanding $L(v, \mathcal{Z}_2)$ in powers of $\mathcal{Z}_1$ we have the expression

$$L = L_o + \mathcal{Z}_1 \cdot L_1 + \mathcal{Z}_1^2 \cdot L_2 \tag{8}$$

where L_0 is given by Eq. (3) whereas L_1 corresponds to a $\mathcal{Z}_1^3$-correction and L_2 to a $\mathcal{Z}_1^4$-correction in the Bethe stopping-power formula. Terms of still higher order are neglected.

The $\mathcal{Z}_1^3$-term, often called the Barkas correction, stems from adiabtic screening effects and receives contributions from both close and distant projectile-electron collisions. An electron gas calculation by Lindhard (1976) and Esbensen (1977) gave the following correction factor

$$\mathcal{Z}_1 \cdot L_1 = \frac{3\pi}{2} \cdot \frac{\mathcal{Z}_1 e^2 \omega_o}{m \cdot v^3} \cdot L_o \tag{9}$$

This result is approximately twice that of previous calculations by Ashley et al. (1972, 1973) and by Jackson and McCarthy (1972), both of which neglect the contribution from close collisions.

Bloch's (1933) universal stopping formula which is valid for all values of $\varkappa_B$ describe the transition between Bethe's quantal and Bohr's (1948) classical stopping formula and contains these in the limits of small and large $\varkappa_B$, respectively. Thus, Bloch's formula contains a correction to the Bethe formula. The correction derives from close collisions only and to first order in $\varkappa_B$ it is given by

$$\mathcal{Z}_1^2 L_2 = -1.202 \left(\frac{\varkappa_B}{2}\right)^2 = -1.202 \cdot \frac{\mathcal{Z}_1^2 v_0^2}{v^2} \tag{10}$$

As pointed out by Lindhard (1976), the Bloch correction is important when comparing p and α measurements.

At low velocities, $v \lesssim v_o \mathcal{Z}_1^{2/3}$, the nuclear as well as the electronic collisions contribute to the slowing-down. The total stopping cross section $S = \mathcal{N}^{-1}\left(-\frac{dE}{dR}\right)$ may be written as

$$S = S_e + S_n \,. \tag{11}$$

Simple theoretical considerations lead to velocity-proportional electronic stopping, and a Thomas-Fermi calculation by Lindhard and Scharff (1961) gives

$$S_e = \xi_e 8\pi e^2 a_o \frac{Z_1 Z_2}{(Z_1^{2/3} + Z_2^{2/3})^{3/2}} v/v_o \,, \; v < v_o Z_1^{2/3} \tag{12}$$

where $\xi_e \sim Z_1^{1/6}$.

In our experimental setup, collisions contributing heavily to the nuclear stopping cause the particles to be scattered out of the angularly narrow forward directed analyzed beam. Hence, only the restricted nuclear-stopping power, denoted by S_n^*, contributes to the measured stopping power. The quantity S_n^* was calculated by Fastrup et al. (1966), and their result may be written as

$$S_n^* = 2.61 \times 10^{-16} \frac{Z_1^2 Z_2^2}{E[\mathrm{keV}]} [M_1/M_2] \, \Phi(\tau) \left[\frac{\mathrm{eV\ cm^2}}{\mathrm{atom}} \right]. \tag{13}$$

Here, the dimensionless quantity $\Phi(\tau)$ is a function of $\tau = N\Delta R \pi a^2$ only, where a is the TF screening radius, $a = 0.8853\, a_o (Z_1^{2/3} + Z_2^{2/3})^{-1/2}$ and $N\Delta R$ the target thickness. Based on the Lenz-Jensen differential-scattering cross section, the function $\Phi(\tau)$ has been calculated numerically and the result is shown in Fig. 1.

Fig. 1: Function used for calculation of the restricted nuclear stopping power S_n^*. For explanation, cf. text.

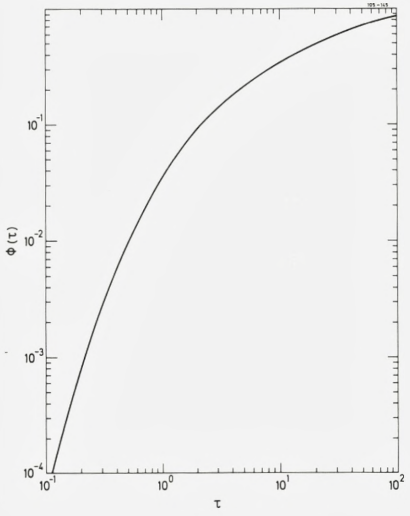

§3. Experimental Procedure and Data Treatment

To perform a systematic investigation of energy loss for light ions in gases, we have measured the stopping powers of nine stopping gases (H_2, He, N_2, O_2,

CO_2, Ne, Ar, Kr, and Xe) for 40-keV to 1-MeV hydrogen and 100-keV to 2.4-MeV helium ions. To cover a large energy region, the measurements were carried out at three different accelerators, an HVEC 2-MV Van de Graaff with magnetic analysis of the energy-degraded beam and a 400-kV Van de Graff and a 100-kV electromagnetic isotope separator both with electrostatic energy analysis. In Table I are shown the energies used at the different accelerators.

Table I

	E_H	E_{He}
2-MV V.d.G.	$0.2 \lesssim E_H \lesssim 1$ MeV	$0.2 \lesssim E_{He} \lesssim 2.4$ MeV
400-kV V.d.G.	$50 \lesssim E_H \lesssim 300$ keV	$100 \lesssim E_{He} \lesssim 300$ keV
100-kV sep.	$35 \lesssim E_H \lesssim 70$ keV	

The overlap of ion energies investigated with the different machines and analyzing techniques is important since it gives a valuable check on the reproducibility of the experimental data.

The experimental setups are shown in Figs. 2 and 3. After acceleration and momentum analysis in a double-focusing sector magnet, the beam is passed through the differentially pumped target region, energy-analyzed by means of an analyzing magnet or an electrostatic analyzer and detected by a solid-state detector.

A. Stopping cell, gas equipment, and pressure measurement.

The stopping cell is a 504 ± 2 mm long, stainless-steel cylinder of 40-mm diameter. Each end of the gas cell is sealed with brass discs with circular, 0.2-mm diameter apertures. By means of a vacuum feed-through, which allows positional adjustments under vacuum, the gas cell is mounted in a 600-mm long cylinder with 2-mm diameter circular entrance and exit apertures. The pressure in the second differential pumping section and the beam lines is typically around $1\text{-}3 \times 10^{-6}$ torr, while the pressure in the first differential pumping region is $P_1 \simeq 10^{-4} P_G$, P_G being the pressure in the gas cell. The purity of the gases was stated by the commercial supplier (Norsk Hydro) to be better than 99.9%.

It is crucial for obtaining reproducible results that the pressure in the gas cell is kept constant. The stability of the target pressure was maintained via a motor-driven, servo-controlled needle valve (Granville-Phillips Company, Series 216). The gas-cell pressure, $0.1 \lesssim P_G \lesssim 2$ torr, was measured with a membrane manometer (C.G.S. Datametrics, type 1083) equipped with a Barocel Pressure Sensor, type 523 H-15. The stated hysteresis was 0.003% and the instrument ranged from zero to two torr with a calibration uncertainty of

0.5%. Owing to the automatic digital readout of the manometer, it was possible to keep a running check of the pressure stability, which was better than 1%.

A mercury thermometer was placed in thermal contact with the vacuum feed-through and thus in contact with the gas cell. The measured temperature was $T = (24.5 \pm 2.5)$°C which, to within the stated accuracy, is identical to the target-gas temperature since the localized heating effects caused by the energy dissipation of the passage of the beam through the gas cell can be shown to give rise to a temperature increase of the target gas of less than 0.7°C. This estimate is based on a steady state. In a previous calculation of the localized heating effect by Bourland et al. (1971) the heat conductivity is neglected. Hence a steady state is not established, and their calculation gave too high an increase of the target temperature.

The target thickness $N\Delta R$ (molecules/cm^2) is found by integrating the local number density $\mu(x)$ along the beam-path length, i.e.

$$N\Delta R = \int_{-\infty}^{\infty} \mu(x)\,dx\,. \tag{14}$$

According to Heinemeier et al. (1975), $\mu(x)$ can be estimated in the following way (*i*) The pressure is constant within the target cell. (*ii*) Outside the target cell the density is found as a sum of two terms (*a*) A constant corresponding to the pressure in the differentially pumped region. (*b*) A varying term which is equal to the target pressure out to a distance equal to the target aperture and then falls off as the inverse square of the distance. Based on this and assuming the ideal gas law we obtain for the target thickness

$$N\Delta R(\text{mol/cm}^2) = A\,\frac{273.15}{273.15+T(^\circ C)}\,\frac{P_G(\text{torr})}{760}\,\ell_{eff}(\text{cm}) \tag{15}$$

where

$$\ell_{eff} = \ell + 2(r_1+r_2) + (\ell_1-\ell)\,P_1/P_G\,. \tag{16}$$

$A = 2.6871\times10^{19}$ (molecules/cm^3) is Loschmidt's number, (ℓ, P_G) and (ℓ_1, P_1) are the length of and the pressure in the gas cell and the first differentially pumped cylinder, respectively, and r_1 and r_2 are the radii of the entrance and exit apertures, respectively. In the present work, the effective length is approximately 0.2% larger than the length of the cell.

B. Energy-analyzing system, detectors, and beam contamination.

The energy-degraded beam was energy-analyzed by a 120-mm radius, 66° cylindrical analyzer (Fig. 2) at the 400-kV Van de Graaff and the 100-kV sepa-

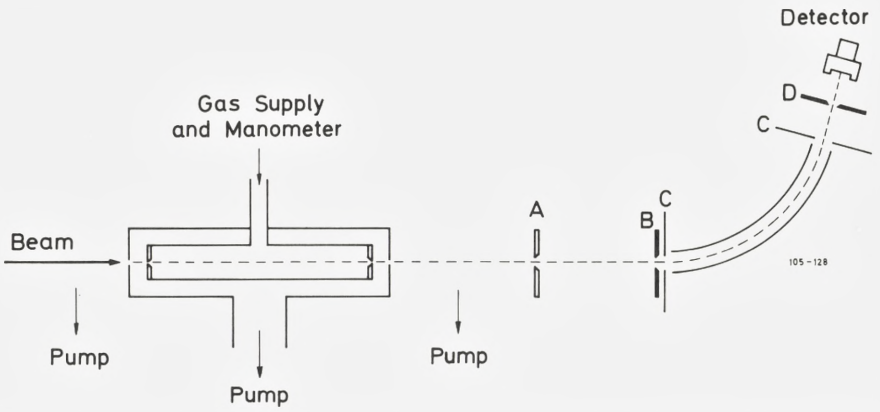

Fig. 2: Experimental setup used at the 400-kV Van de Graaff and at the 100-kV isotope separator.

rator. The analyzer electrodes are 4.9 mm apart and connected to a ~ 12.5 kV symmetric high-voltage supply, which corresponds to the deflection of 0.3 MeV singly charged particles. Apparatures A and B, two 1-mm-wide slits, and aperture D, a 0.42-mm-wide slit, are beam-defining, while the apertures C are used to scrape off scattered halos from the beam.

By extrapolation of the FWHM of the measured energy-loss distributions to zero pressure, we found an energy-independent relative energy resolution (FWHM/E_i) of 0.74%.

The energy calibration was carried out at the 400-kV Van de Graaff accelerator by means of the $^{19}F(p,\alpha)^{16}O$ reaction ($E_{res} = 340.46 \pm 0.04$ keV; $\Gamma = 2.4 \pm 0.2$ keV) as the primary standard. The calibration was checked at the 100-kV isotope separator, at which the accelerator voltage was measured directly by a high-voltage probe to within ± 150 V. The measured beam energies and acceleration voltages agreed within the stated accuracy. The analyzer linearity was investigated in connection with measurements of lithium stopping powers (Andersen et al. 1978). Li^+ and Li^{++} beams emerging from krypton and xenon targets much thicker than the mean-free path for charge-exchange processes were analyzed and requiring a difference of a factor of two in the reference voltages, it was found that the measured energies for Li^+ and Li^{++} agreed within ± 0.2%. The uncertainty in the absolute calibration of the electrostatic analyzer is estimated to be 0.4%.

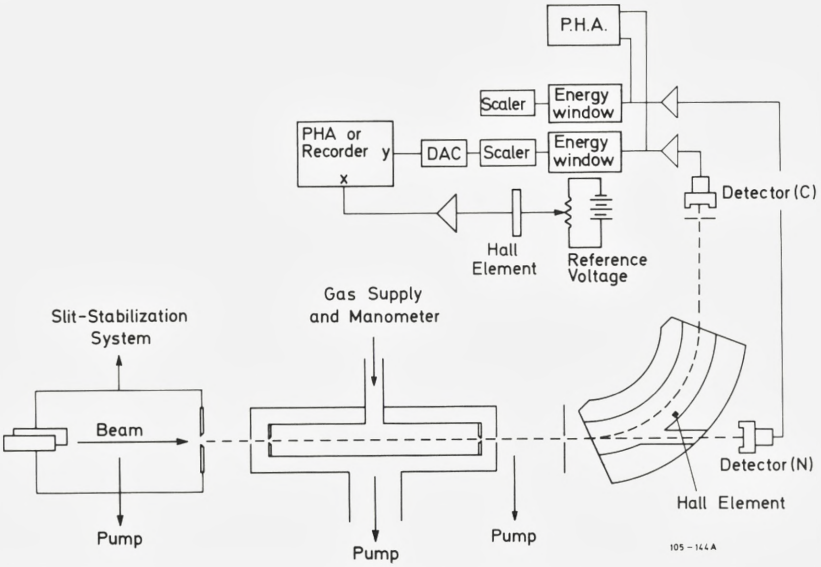

Fig. 3: Experimental setup used at the 2-MV Van de Graaff accelerator.

At the 2-MV Van de Graaff, the energy-loss distributions were analyzed by a 40-cm radius, 90° double-focusing sector magnet (Fig. 3). The magnetic field was measured with a Hall probe, the integral linearity of which was found to be better than 0.5%. The differential linearity of the Hall probe checked by a NMR fluxmeter was better than 0.1%. Tantalum slits with openings of 0.45 mm were placed immediately in front of detector C, and we found a relative energy resolution (FWHM/E_1) of 0.10%. The incoming beam was momentum-analyzed in a 72° double-focusing sector magnet with an energy dispersion of $\Delta E/E \sim 7 \times 10^{-5}$. Hence, in order to obtain a position-stable beam at the target, we used a slit-stabilization system (shown in Fig. 3), which is a feed-back system consisting of two vertical stainless-steel "knives" in front of the target chamber and a set of vertical deflection plates at the exit of the bending magnet.

For the present stopping-power and straggling measurements, the use of solid-state surface-barrier detectors is important. From the detector energy spectrum, it was possible (*i*) to reveal the presence of low-energy, slit-edge-

scattered particles and (*ii*) to identify a possible oxygen-beam contaminant with the same kinetic energy as a primary helium beam. The contaminant is formed by electron loss between the base plate and the bending magnet from a $^{16}O^{+}$ beam accelerated together with He^{+}. Due to the higher pulse-height defect (Steinberg et al. 1972) of the oxygen than that of the helium beam, it is possible to separate the oxygen and helium beams in the pulse-height spectrum. Actually, only once, just after reloading the ion source and under bad vacuum conditions, we did observe any substantial contamination.

C. Electronic equipment.

At the 400-keV Van de Graaff and the separator, use of the electrostatic analyzer for the energy analysis enabled us to apply the multiscaling-sweep technique previously employed for lateral spread measurements (Knudsen et al. 1976). A single-channel window was positioned around the main peak in the energy spectrum from the solid-state detector, and the selected signal was fed to the multichannel analyzer, running in multiscaling mode. After adequate biasing and amplification, the horizontal sweep voltage of the multichannel scope was used as an external reference signal for the analyzer high-voltage power supply. The energy window of the analyzer was thus swept over the energy distribution of the beam synchronously with the multiscaler. Through a simultaneous measurement of the reference voltage for the electrostatic analyzer with a digital voltmeter, the energies corresponding to the upper and lower ends of each sweep were determined, and the energy distribution appeared directly as a spectrum in the multichannel analyzer without transformation. Using this sweep technique we did not need any beam normalization, while the experimental equipment used at the 2-MV Van de Graaff and shown in Fig. 3 utilized detector N as a normalizing device.

D. Data treatment.

With a few exceptions, the pressure in the stopping cell was chosen to make the target thickness satisfy the following criterion,

$$\varkappa_V = (\Omega/T_m)^2 = N\Delta R \frac{\pi Z_1^2 Z_2 e^4}{4E^2} (M_1/m)^2 > 10 . \tag{17}$$

According to Bohr (1948) and Vavilov (1957), Gaussian energy-loss distributions are obtained when inequality (17) is fulfilled. This was confirmed by the measured energy spectra. In the inequality (17), Ω is the standard deviation of the

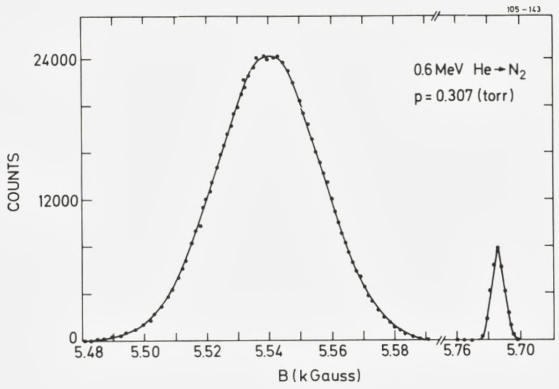

Fig. 4: Momentum distribution of an incident 600-keV beam and the same beam emerging from an N_2 target.

energy-loss distribution, approximated by the Bohr formula (Bohr 1948), $\Omega_B^2 = 4\pi Z_1^2 Z_2 e^4 N \Delta R$, and T_m is the maximum energy transfer in a single collision with an electron.

With the analyzing magnet, momentum spectra were obtained at each beam energy with and without gas in the stopping cell. A typical momentum distribution is shown in Fig. 4. From the energy-versus-field relation, the energy loss is given by

$$\Delta E = E_i \cdot \frac{\Delta B}{B_i}\left(2 - \frac{\Delta B}{B_i}\right), \tag{18}$$

where $\Delta B/B_i$ is the relative reduction in magnetic field. This shows that for small changes ($\Delta B/B_i \ll 1$), the B axis can be considered as an energy axis. Alternatively, the mean energy loss and the standard deviation are determined from

$$<\Delta E> = E_i - (E_1 + E_2)/2 \tag{19}$$

and

$$\Omega_E = \frac{E_2 - E_1}{2\sqrt{2 \log 2}} \tag{20}$$

where E_1 and E_2 are the energies corresponding to the half-maximum positions for the momentum distribution. Formula (19) is preferable to formula (18) in a calculation of $<\Delta E>$ due to the larger uncertainty in the determination of the peak position compared to the HWHM positions of the distribution.

With the electrostatic analyzer, determination of the primary-beam energy was more problematic as transmission of the beam without gas in the cell would damage the detector. Hence, the following procedure was adopted: At each

selected beam energy, energy-loss spectra for all gases were measured without changing any of the accelerator settings which may influence the energy, and, at least for one particular gas, energy distributions were measured at three different pressures, corresponding to an energy loss of approximately 5, 9, and 13%. A straight line was fitted to the three measured average energies versus target pressure, and the extrapolation to zero pressure gave a preliminary value of the unattenuated beam energy. Provided the stopping power in question was energy-independent, this value was correct. This not being the case, the preliminary primary energies were used to calculate preliminary stopping powers, and primary energies were obtained through iteration. The uncertainty in the determination of $<\Delta E>$ from formula (19) was 1.5% (2σ). Finally, experimental stopping cross sections are obtained as

$$S_o = \frac{<\Delta E>}{N\Delta R} . \tag{21}$$

E. Stopping cross sections and corrections.

The electronic-stopping cross section S_e is derived from the observed stopping cross section S_o through subtraction of the restricted nuclear-stopping cross section S_n^* given by formula (13), i.e.,

$$S_e = S_o - S_n^* . \tag{22}$$

For all combinations of target, projectile, and energy, the correction for nuclear collisions is less than 0.5%. However, the correction has been taken into account whenever it exceeds 0.1%.

The energy attributed to the measured stopping cross section is to first order in $<\Delta E>/E$ given by

$$E_{av} = E_i - <\Delta E>/2 . \tag{23}$$

An expansion by Andersen et al. (1966) of $S(E_{av})$ in powers of $<\Delta E>/E$ gives a quadratic correction term to the stopping cross section. As the relative energy loss was always less than 15%, this correction was less than 0.1% and hence omitted.

F. Experimental accuracy.

First, we summarize the quoted systematic errors stemming from uncertainties in the incident-energy E_i(0.3-0.5%), the differential (0.1%), and the integral

(0.5%) linearity of the Hall element, the linearity (0.2%) and the absolute calibration (0.4%) of the electrostatic analyzer, the effective target length (0.4-0.6%) and, finally, the calibration of the membrane manometer (0.5%).

The non-systematic errors originate from uncertainties in the absolute gas temperature (<1%), the pressure in the gas cell (<1%), the HWHM for the degraded energy-loss distribution due to counting statistics (1.5%), and the determination of the length of the sweeping interval (0.3%).

From the uncertainties, all of which correspond to two standard deviations (2σ), it is concluded that the stopping powers are measured to within an uncertainty of 2.5% (2σ).

§4. Experimental Results and Comparison with other Data

The experimental electronic-stopping powers S_e for hydrogen and helium ions in H_2, He, N_2, O_2, Ne, Ar, Kr, Xe, and CO_2 are plotted in Figs. 5-18 as functions of E_{av}. In the figures, the present results have been compared with most other published hydrogen and helium energy-loss data. The scatter of our data points is consistent with the estimate of the measuring accuracy given above.

A. Hydrogen stopping powers.

Recently Andersen and Ziegler (1977) published tabulations of hydrogen stopping powers for all elements in the energy range 10 keV $<(E/\text{amu})<$ 20 MeV. These semi-empirical stopping-power fits are plotted in Figs. 5-13. From the figures we first note that for most of the targets used, good agreement exists between the Andersen and Ziegler semi-empirical stopping-power fits and the present experimental results for energies $E \gtrsim 100$ keV. However, the semi-empirical fits have a tendency of being slightly low around the stopping-power maximum, and for Xe targets, the fit to our data as well as to those previously published is rather poor over a broad energy range. The present results agree within the stated accuracy with the averaged S_H-values found by Reynolds et al. (1953), the accuracy of which is 2-4% (2σ), while the data obtained by Phillips (1953) are systematically $\sim 15\%$ lower. Since Phillip's results are included in the data on which the tabulations by Andersen and Ziegler are based, their curve appears to be too low for energies $E \lesssim 100$ keV.

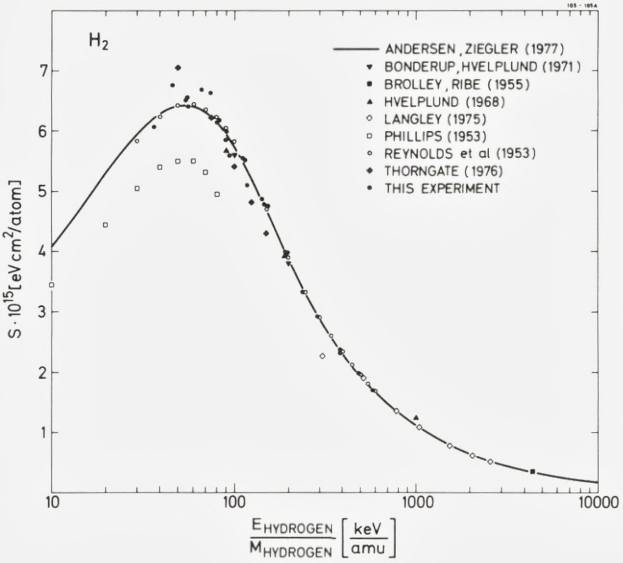

Fig. 5: Stopping-power results for hydrogen in H_2.

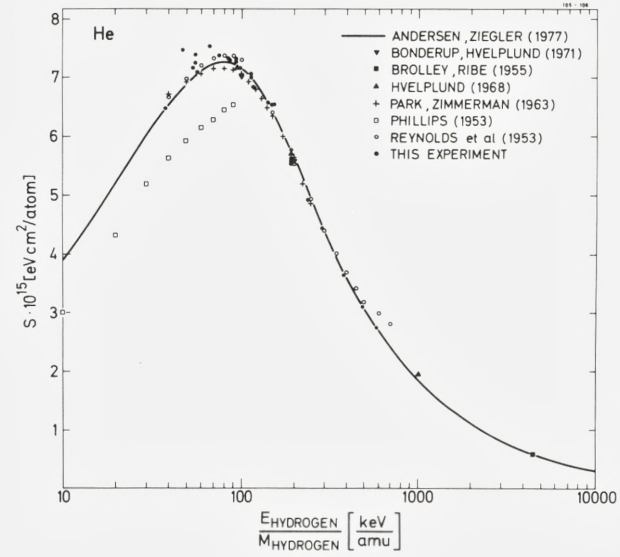

Fig. 6: Stopping-power results for hydrogen in helium.

Fig. 7: Stopping-power results for hydrogen in N_2.

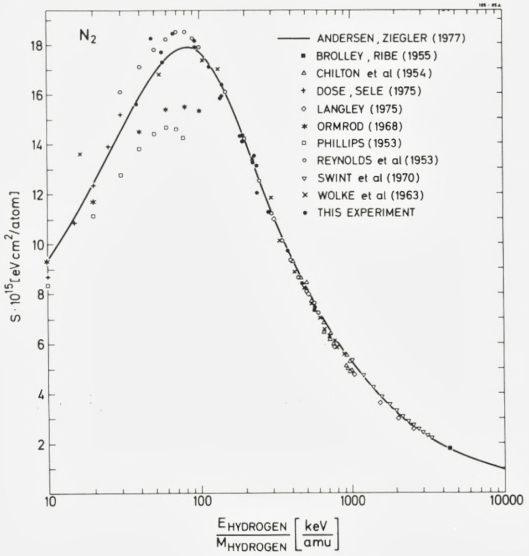

Fig. 8: Stopping-power results for hydrogen in O_2.

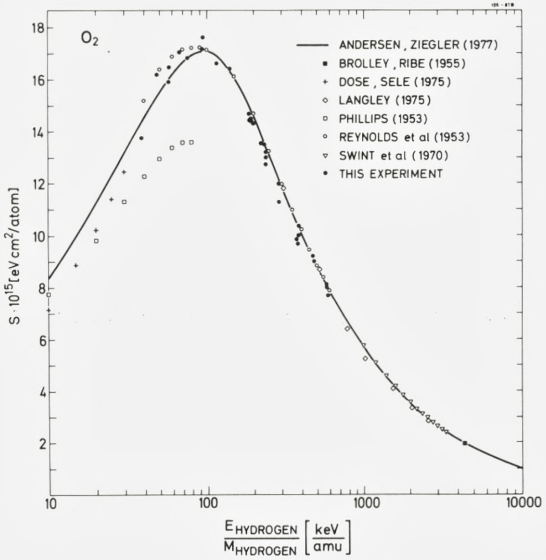

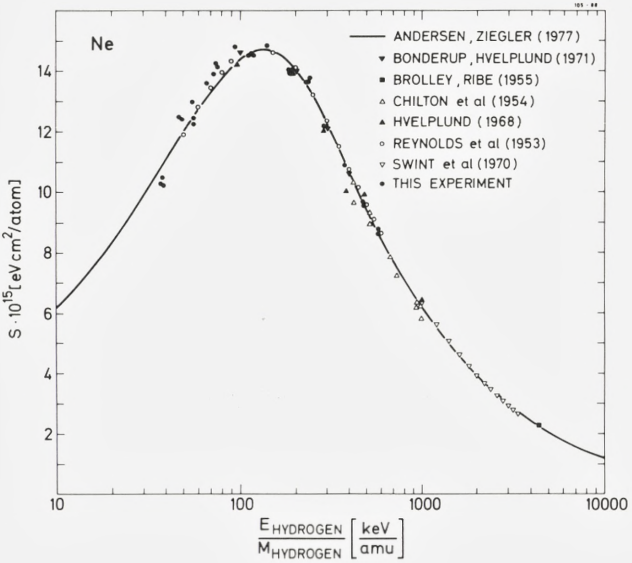

Fig. 9: Stopping-power results for hydrogen in neon.

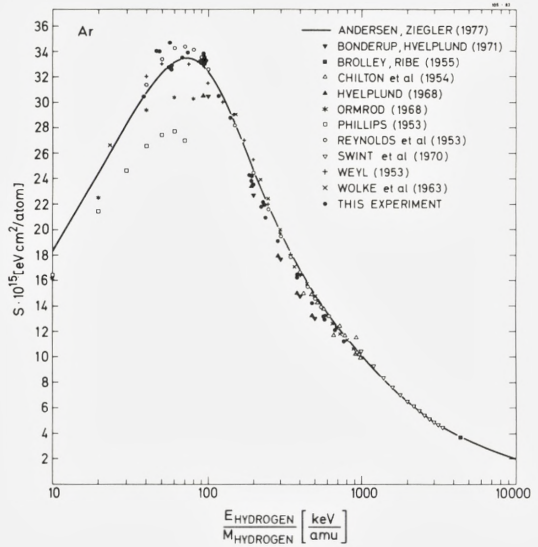

Fig. 10: Stopping-power results for hydrogen in argon.

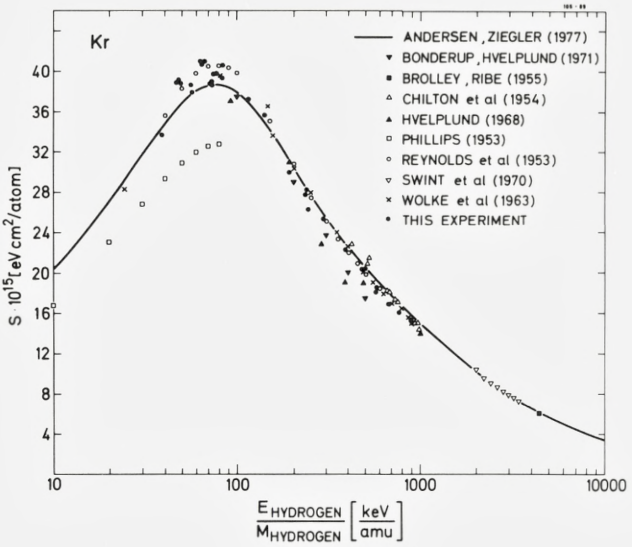

Fig. 11: Stopping-power results for hydrogen in krypton.

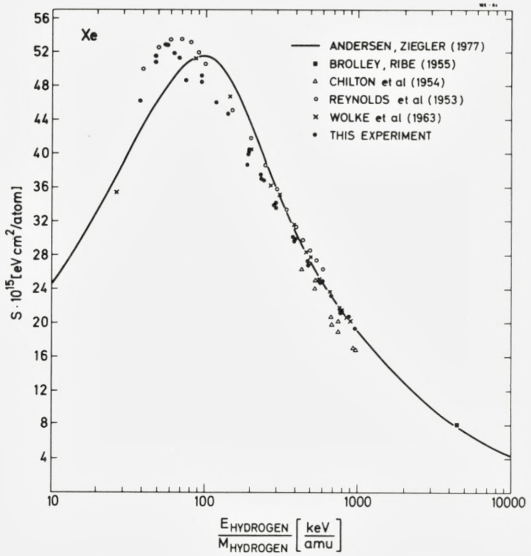

Fig. 12: Stopping-power results for hydrogen in xenon.

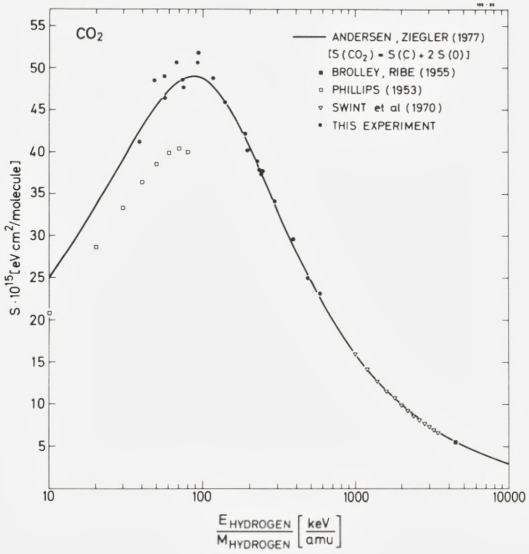

Fig. 13: Stopping-power results for hydrogen in CO_2.

B. Helium stopping powers.

Very recently, Ziegler (1978) published helium stopping-power tabulations similar to those of Andersen and Ziegler (1977) mentioned above. As the present experimental results are included in Ziegler's helium-data base, they constitute no independent check of these tables. Hence the tabulations are not included in Figs. 14-18. Nor are the polynomial fits made by Ziegler and Chu (1974) since for the present gases, these fits are identical to the averaged S_{He} values of the Baylor group (see below) as plotted in Figs. 14-18.

With a setup more or less equivalent to the present one, the Baylor group, Bourland, Chu, and Powers (1971) and Chu and Powers (1971) have made a systematic investigation of α-particle stopping cross sections in gases. The stated accuracy of their measurements ranges from 1.5% to 3% (2σ). As can be seen from the figures, the measurements performed by the Baylor group are higher by 1-6% than the present S_{He} results. This difference is not understood at present. However, it should be pointed out that the Baylor group employed a non-energy dispersive detector (a Faraday cup), and hence could not reveal the presence of slit-edge-scattered particles and/or a possible oxygen contamination of the helium beam. As they have not published the straggling results, it is not possible to disclose whether beam contamination and/or pressure fluctuations were significant. Finally, as a McLeod gauge was used, the pressure could not

be checked continuously. However, it should be noted that the Baylor group performed independent measurements in a sealed gas cell, using a solid-state detector. These measurements ($\pm 5.4\%$ to $\pm 6.7\%$ (2σ)) were not as accurate as the differentially pumped gas-cell measurements but they did agree with the latter to within the stated accuracy.

In this connection, it should be noted that the reliability of the present measurements is enhanced due to the fact that the stopping cross sections for both hydrogen and helium ions were measured in the same gases, and the present S_H data agree with most other S_H data.

The stopping cross sections by Hvelplund (1968, 1971) for helium in H_2, He, O_2, and Ne are systematically 10-15% below the present data. This discrepancy is difficult to understand since Hvelplund's equipment was similar to that used here. However, it is fair to mention that the data by Fastrup et al. (1968), and the lithium stopping power results by Andersen et al. (1978) lie 10-16% and 20% above Hvelplund's results, respectively. Hvelplund's proton stopping-power and straggling data (Bonderup and Hvelplund 1971) are in much better agreement with our present data.

Using a natural α-emitter source and a solid-state detector, Hanke and Bichsel (1970), Palmer (1966), and Rotondi (1968) measured range-energy relations for α particles in Ar, H_2, CO_2, N_2, and O_2. Hanke and Bichsel made a thorough data evaluation, taking into account corrections for multiple scattering, discrete energy loss (Lewis correction), undetected energy losses in the detector gold-surface layer, and adjoining dead layer and energy loss due to self-absorption in the source head. Thus, by differentiating the range-energy curve, they determined the stopping cross section for helium in argon with a claimed accuracy of 0.2% for $E_{He} > 2$ MeV, decreasing to 1.5% for $E_{He} \sim 1$ MeV. Palmer and Rotondi did not correct their range-energy results, and this may explain why their stopping-power results, especially around the maximum, deviate significantly from the present data.

By using an ^{241}Am α source and a solid-state detector, Kerr et al. (1966) and Wenger et al. (1973) have measured S_{He} at energies $0.3 \lesssim E_{He} \lesssim 5$ MeV by either varying the pressure in the absorber chamber between 0 and 720 mm Hg (Kerr et al. 1966) or by changing the distance between source and detector with the gas held between them kept at a pressure of 2.54 torr above atmospheric pressure (Wenger et al. 1973). Since there is a large uncertainty in the energy, which they attribute to the measured stopping power due to the large energy loss and as the above corrections to the stopping power are not taken into account, it is evident that these measurements are vitiated by large uncertainties. This is also the case for the data by Ramirez et al. (1969) for similar reasons.

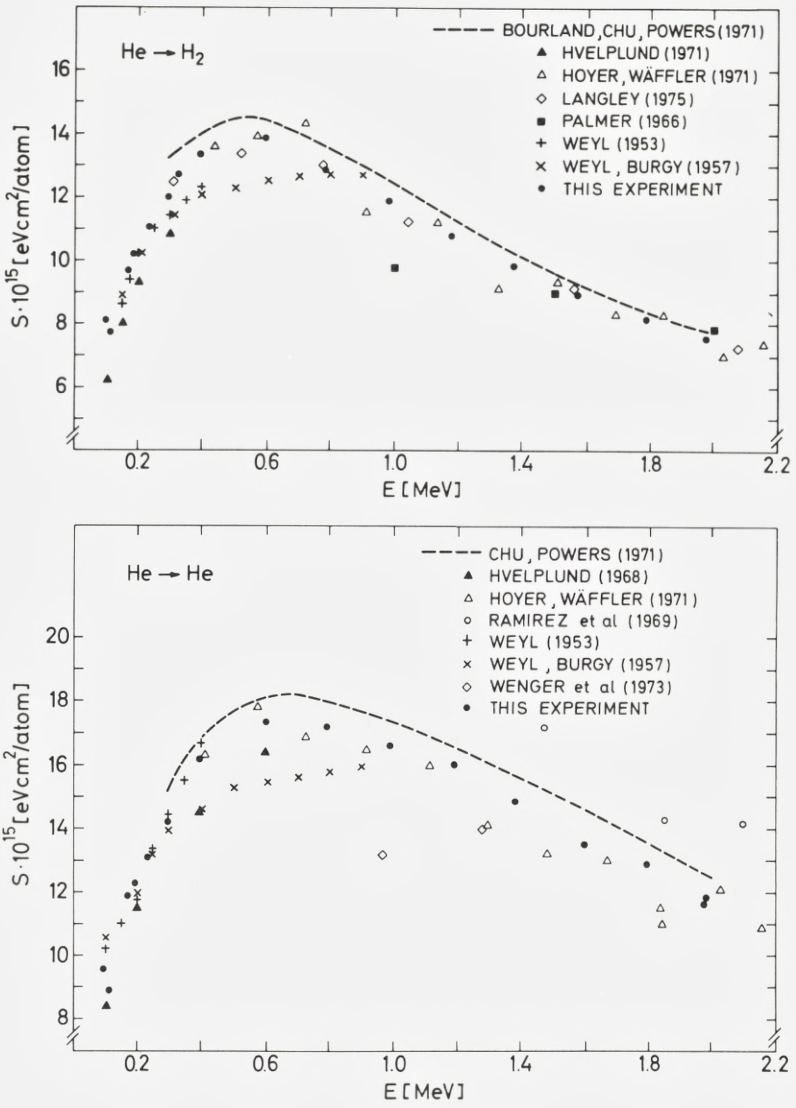

Fig. 14: Stopping-power results for helium in H_2 and He.

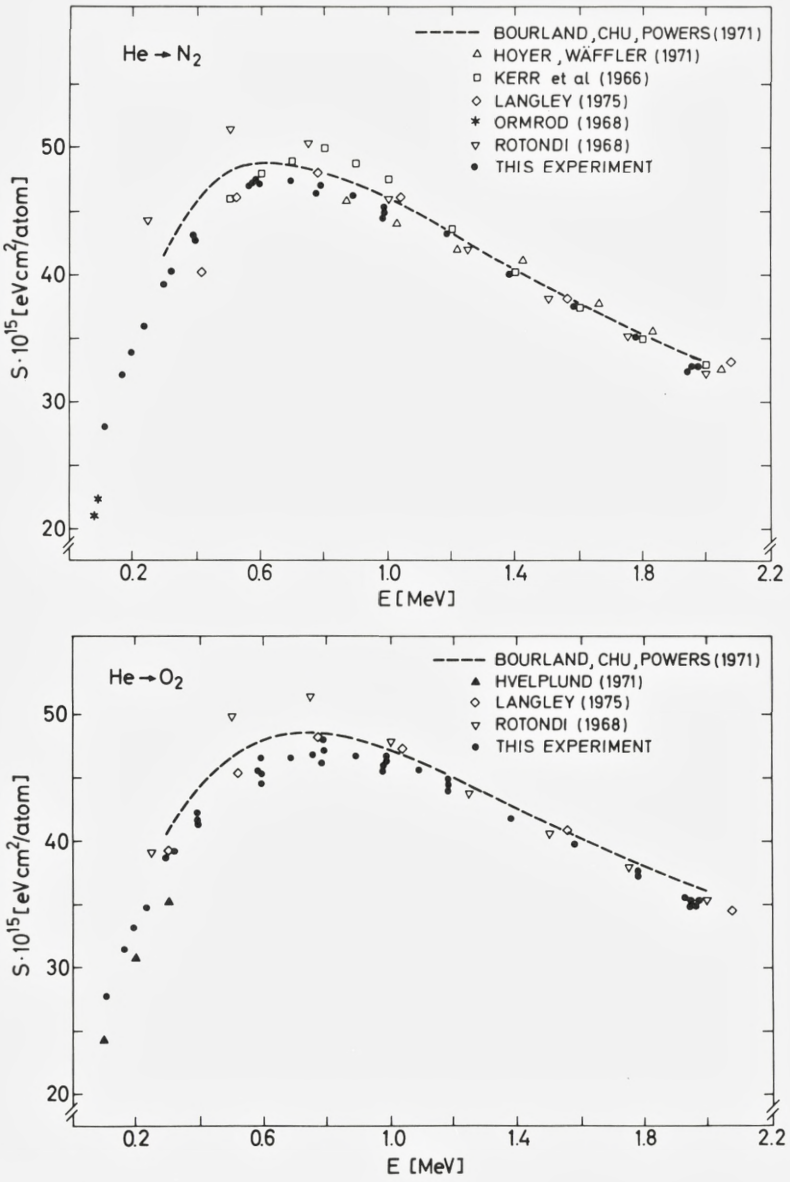

Fig. 15: Stopping-power results for helium in N_2 and O_2.

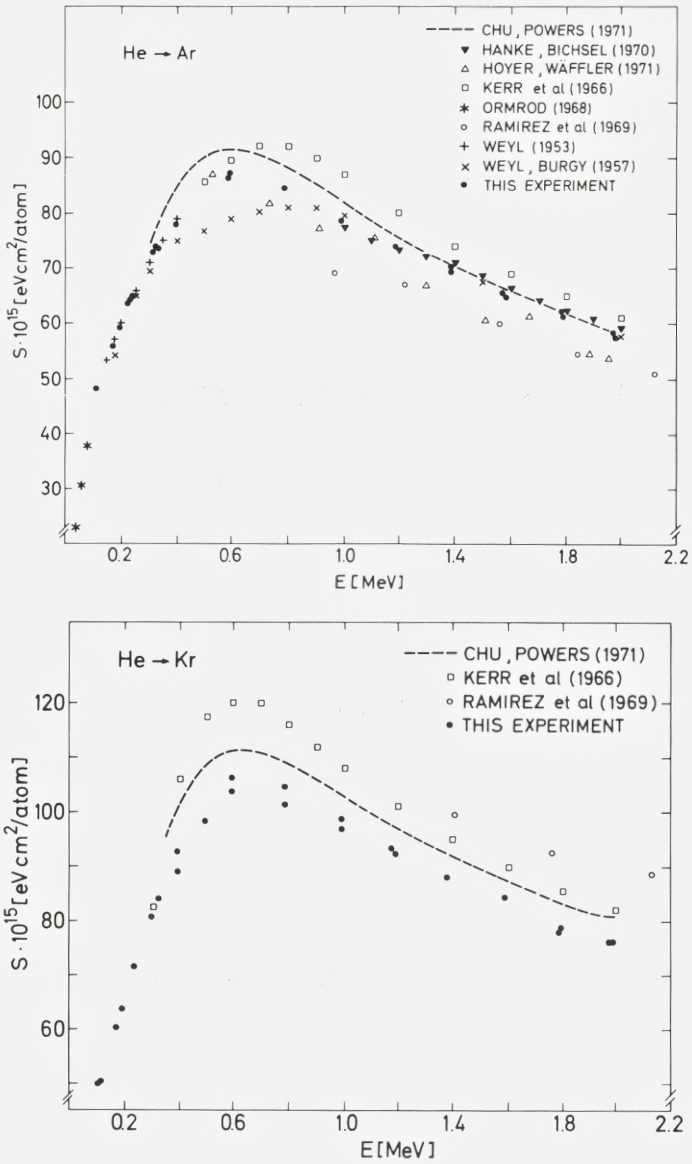

Fig. 16: Stopping-power results for helium in argon and krypton.

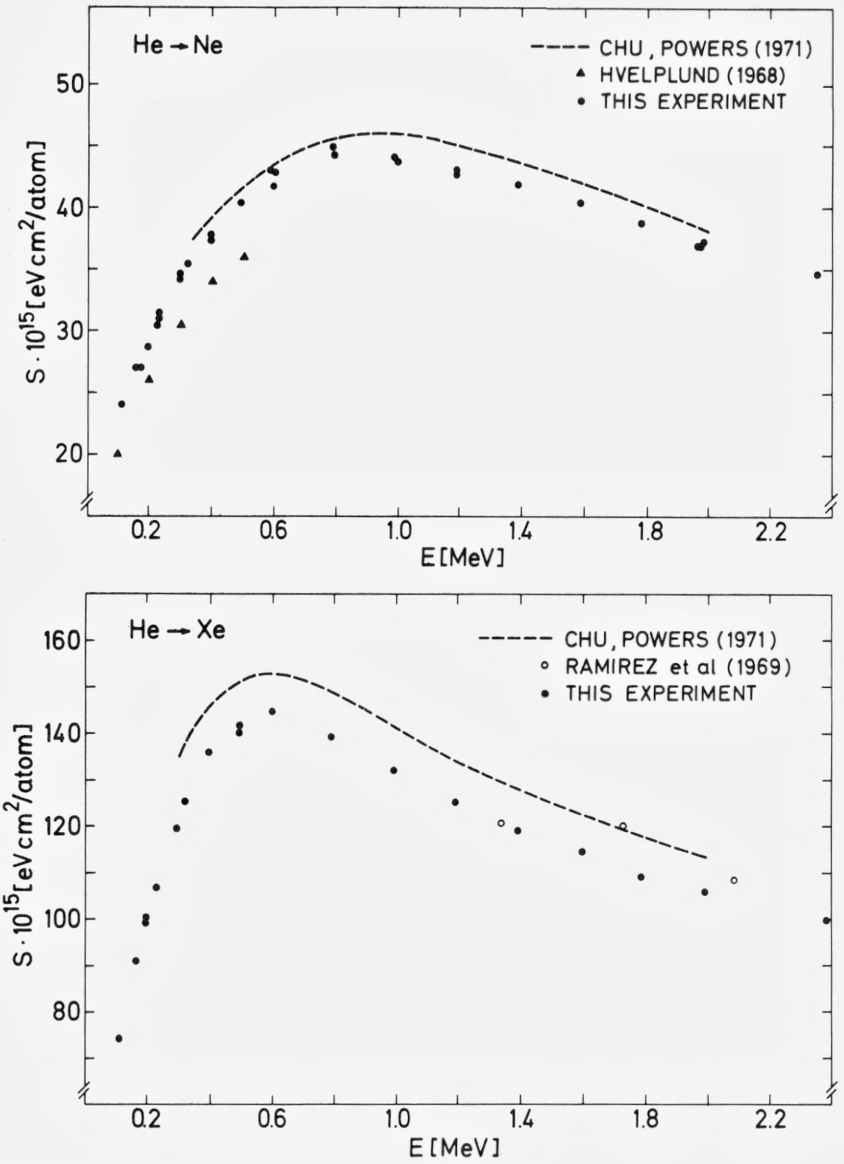

Fig. 17: Stopping-power results for helium in neon and xenon.

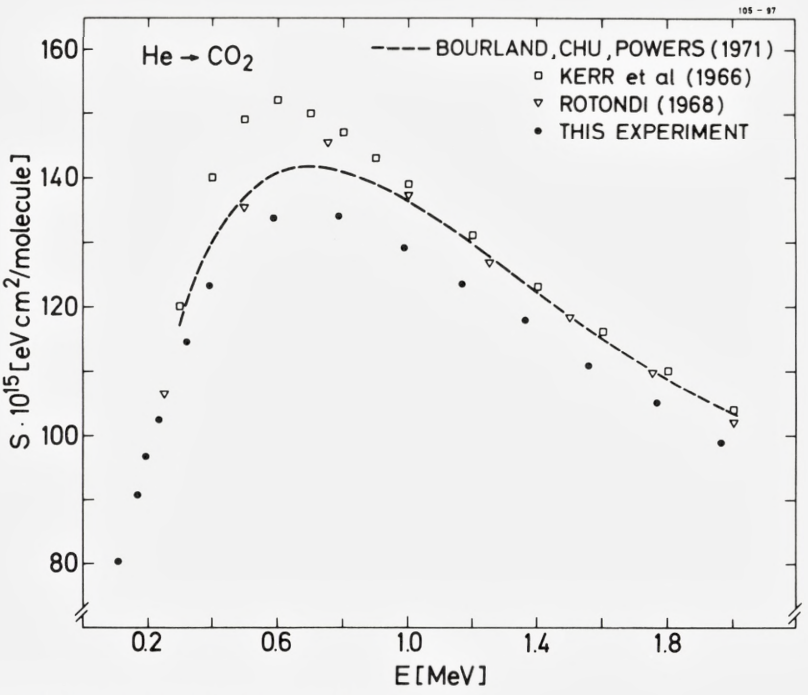

Fig. 18: Stopping-power results for helium in CO_2.

§5. Comparison with Theory

A. Shell corrections and I values.

Before making any comparison of the experimental results with the calculations based on the Lindhard-Scharff model and its refinements, we should emphasize that the region of validity of a perturbation treatment for a free electron gas is restricted to $\varkappa_B < 1$ or $v > 2v_o Z_1$ (Bonderup 1967), i.e., to hydrogen and helium energies higher than ~ 100 keV and ~ 1600 keV, respectively. Therefore any comparison between the present helium stopping powers and existing calculations should be taken with some reservation.

As argued in §2, it is advantageous to apply the so-called shell corrections C/Z_2 rather than $L(v, Z_2)$ in a detailed comparison between theory and experiment. Introducing Bichsel's (1964) reduced stopping-power variable,

$$X = \log\left(\frac{2mv^2}{1-(v/c)^2}\right) - \left(\frac{v}{c}\right)^2 - 1/\mathcal{Z}_2 \frac{mv^2}{4\pi e^4 \mathcal{Z}_1^2} S_{\text{exp}} \ , \tag{24}$$

we may deduce empirical shell corrections from the experimental hydrogen stopping powers using formulas (2) and (3) as

$$(C/\mathcal{Z}_2)^*_{\text{exp}} = X^H_{\text{exp}} - \log I \, . \tag{25}$$

As will be discussed later the shell corrections deduced from this formula are not genuine shell corrections and are therefore labelled with an asterix.

In Figs. 19 and 20, experimental shell corrections $(C/\mathcal{Z}_2)^*$ obtained from formula (25) are presented as a function of energy. The I values used are those extracted by Andersen and Ziegler (1977) from their fits to previously published data. Comparison is made to Bonderup's (1967) theoretical calculations $(C/\mathcal{Z}_2)_B$ and to the empirical shell corrections by Andersen and Ziegler. As an indication of the sensitivity of $(C/\mathcal{Z}_2)^*$ to uncertainties in the S_H data, the distance between the dashed line "3% effect on stopping" and the zero line gives the change in $(C/\mathcal{Z}_2)^*$ due to a 3% change in stopping power. An increase in stopping power gives a lower X value and hence a lower $(C/\mathcal{Z}_2)^*$ value.

From Figs. 19 and 20 it is observed that the experimental $(C/\mathcal{Z}_2)^*$ data deviate significantly from Bonderup's shell corrections $(C/\mathcal{Z}_2)_B$ both in size and shape (see, e.g., H $\rightarrow$ Ne). Until recently, it was believed that this discrepancy was due to a defiency in the theoretical model in the energy region discussed here. However, all possible deviations from formulas (2) and (3) such as higher-order $\mathcal{Z}_1$ corrections are automatically included in the empirical $(C/\mathcal{Z}_2)^*$ values. According to formula (8), the correct shell correction is determined from

$$(C/\mathcal{Z}_2) = X^H_{\text{exp}} - \log I + \mathcal{Z}_1 L_1 + \mathcal{Z}_1^2 L_2 \, . \tag{26}$$

Therefore the experimental $(C/\mathcal{Z}_2)^*$ proton values in Figs. 19 and 20 should be compared to the following "apparent" theoretical shell-corrections

$$(C/\mathcal{Z}_2)^*_{th} = (C/\mathcal{Z}_2)_B - (L_1 + L_2) \, . \tag{27}$$

In calculating $(C/\mathcal{Z}_2)_{th}{}^*$, we have used the Bloch expression, formula (10), for L_2. According to the discussion in connection with formula (9), the Barkas correction L_1 has been set equal to twice the quantity given by Jackson and McCarthy (1972)

$$L_1 = 2L_1{}^{JM} = 2\frac{F\left(\frac{v}{v_o}\frac{1}{\mathcal{Z}_2^{1/2}}\right)}{\mathcal{Z}_2{}^{1/2}} L_o \, . \tag{28}$$

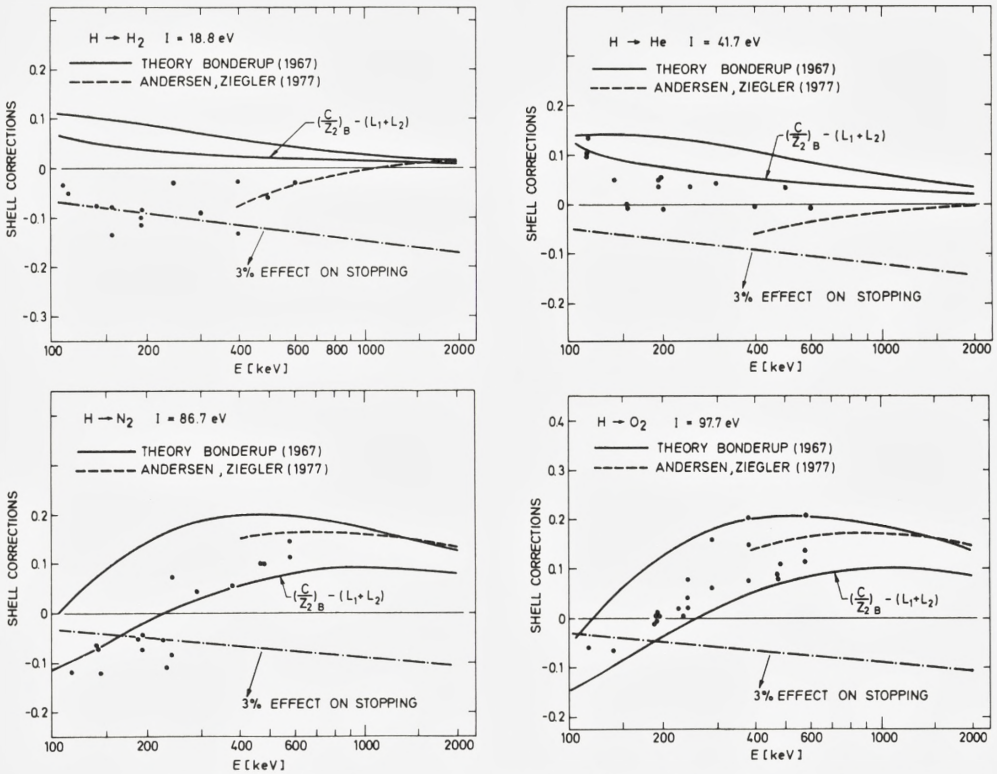

Fig. 19: Experimental shell corrections for H_2, He, N_2, and O_2 obtained from Eq. (25) (points), compared with Andersen and Ziegler's semiempirical fit (dashed), Bonderup's theoretical values and those values corrected for higher-order Z_1 effects, according to Eq. (27). The I values are those given by Andersen and Ziegler (1977).

In calculating L_1 for the heavier elements, we have extrapolated $L_1{}^{JM}$ slightly outside the stated region of validity given by $\frac{1}{Z_2^{1/2}} \frac{v}{v_o} \gtrsim 0.8$. Theoretical shell corrections obtained from formula (27) are also plotted in Figs. 19 and 20.

In the cases of N_2, Ne, Ar, and Xe, the corrected values $(C/Z_2)_{th}^* = (C/Z_2)_B - (L_1 + L_2)$ show perfect agreement with the experimental values $(C/Z_2)^*$. For H_2, He, O_2, and Kr, the energy dependence of the experimental data $(C/Z_2)^*$ agrees much better with the energy dependence of the corrected values

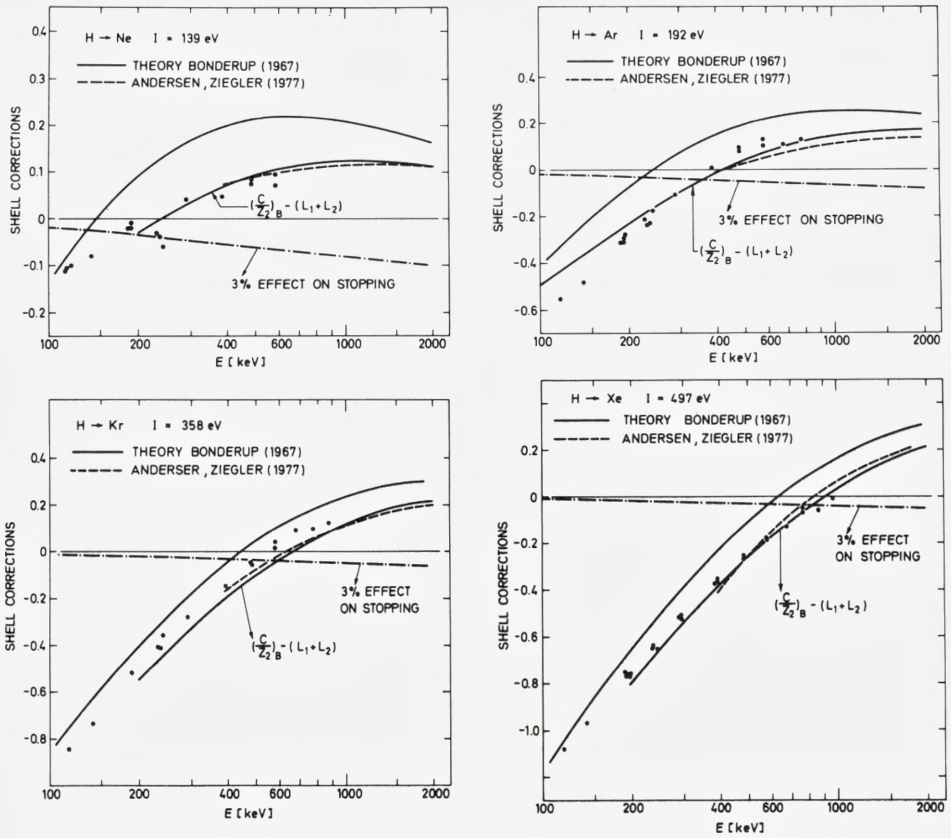

Fig. 20: Experimental shell corrections for Ne, Ar, Kr, and Xe. See caption to Fig. 19 for further explanation.

$(C/Z_2)^*_{th} = (C/Z_2)_B - (L_1 + L_2)$ than with that of $(C/Z_2)_B$. However, there is a systematic shift in the absolute value between $(C/Z_2)^*$ and $(C/Z_2)^*_{th}$, which may originate in the choice of I value. A change of I to $I - \Delta I$ changes the experimental $(C/Z_2)^*$ data by the additive amount $\Delta I/I$. In this way, experimental I values are determined from the present data. In Table II, the resulting experimental ionization potentials are compared with those given by Andersen and Ziegler (1977) and Chu and Powers (1972).

Table II

I(eV)	H_2	He	N_2	O_2	Ne	Ar	Kr	Xe
Present results	17.6	40.7	86.7	102.1	139	194	376	497
Andersen-Ziegler	18.8	41.7	86.7	97.7	139	194	358	497
Chu-Powers			92.4	110	160	207	403	529

It is concluded that the present I values, which constitute an independent check of the Andersen and Ziegler I values, are in good agreement with these, while the theoretical I values by Chu and Powers are systematically too high.

Above, we used the experimental shell corrections $(C/\mathcal{Z}_2)^*$ as a standard and corrected Bonderup's theoretical calculations $(C/\mathcal{Z}_2)_B$ for comparison. Andersen et al. (1977) employed $(C/\mathcal{Z}_2)_B$ as a standard and corrected $(C/\mathcal{Z}_2)^*$ by adding (L_1+L_2) for comparison. The reason for our approach is that in the present energy region, we are not able to determine L_1 and L_2 experimentally as was done by Andersen and coworkers and hence we could not obtain experimentally determined genuine shell corrections with which to compare the theoretical $(C/\mathcal{Z}_2)_B$ results.

A different approach is to use the empirical fits for L_1 and L_2 extracted from the measurements by Andersen et al. (1977) and denoted by L_1^A and L_2^A, respectively. For $\mathcal{Z}_2 > 10$, good agreement is found between $(C/\mathcal{Z}_2)_B - (L_1+L_2)^A$ and formula (27) shown in Figs. 19 and 20, while the agreement becomes increasingly unsatisfactory for $\mathcal{Z}_2 < 10$. As Andersen and coworkers measured stopping powers of Al, Cu, Ag, and Au, their empirical fits for L_1 and L_2 should be employed only for $13 \lesssim \mathcal{Z}_2 \lesssim 79$, in which case they give results which are consistent with the present data.

Concerning Andersen and Ziegler's (1977) "fitted shell corrections", $(C/\mathcal{Z}_2)^{AZ}$, all higher-order $\mathcal{Z}_1$ contributions are piled onto these, and $(C/\mathcal{Z}_2)^{AZ}$ should therefore be compared with the present results $(C/\mathcal{Z}_2)^*$ or with $(C/\mathcal{Z}_2)_B - (L_1+L_2)$. In the cases of Xe, Kr, Ar, Ne, and O_2, there is good agreement between $(C/\mathcal{Z}_2)^{AZ}$ and the present data $(C/\mathcal{Z}_2)^*$. For N_2, the curve for $(C/\mathcal{Z}_2)^{AZ}$ is somewhat higher than $(C/\mathcal{Z}_2)^*$, while for H_2 and He, the fit $(C/\mathcal{Z}_2)^{AZ}$ deviates both in magnitude and energy dependence from the present results. If Andersen and Ziegler had based their fit for H_2 and He not on the scarse and scattered available experimental data points but had extrapolated the shell-correction fit obtained for other elements with $\mathcal{Z}_2 \geq 3$ to the cases of H_2 and He, the present H_2 and He results would have agreed with the general trend on the $(C/\mathcal{Z}_2)^{AZ}$ curves.

B. Experimental determination of the Z_1^3 correction.

We assumed above that the Barkas and the Bloch corrections were given by the formulas (28) and (10), respectively. Andersen et al. (1977) have demonstrated that this is approximately correct for $7 \lesssim v/v_o \lesssim 12$. In our case we can extract information on the higher order Z_1 terms only when the helium ions are known not to carry electrons in a bound state. Equilibrium charge-state measurements show that this is the case for $E_{He} \gtrsim 1.6\text{-}2$ MeV. Furthermore, from measurements with hydrogen and helium ions only, it is not possible to distinguish between Z_1^3 and Z_1^4 corrections. However, based on the results by Andersen et al. (1977), it seems reasonable to assume that L_2 is given approximately by the Bloch expression, formula (10). As follows from Eqs. (8) and (24), experimental L_1 values may then be extracted from the formula

$$L_1^{exp} = X_H^{exp} - X_{He}^{exp} - 3L_2 \,. \tag{29}$$

The uncertainties in L_1^{exp} are calculated under the assumption that the uncertainty in L_2 is $\sim 20\%$.

In Fig. 21, experimental L_1 values for H_2, N_2, O_2, Ne, Ar, and Xe are compared with the theoretical estimate for L_1 given by Eq. (28), which is a good

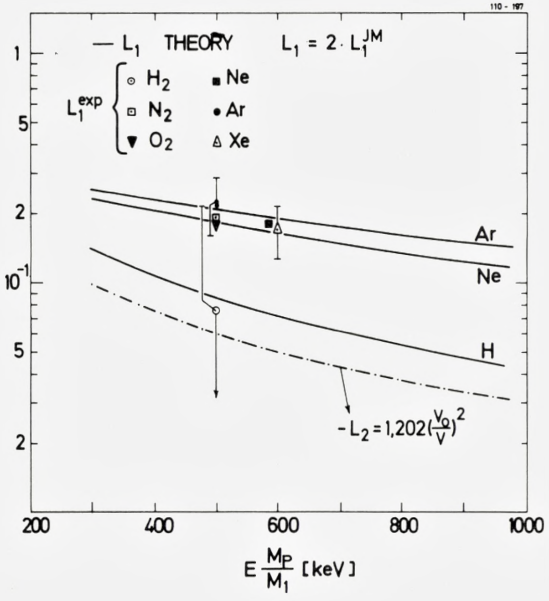

Fig. 21: Experimental results for the Z_1^3 factor L_1 obtained from Eq. (29). Theoretical curves for L_1 (solid) and L_2 (dot-and-dash) are Eqs. (28) and (10) respectively.

approximation to the results of Lindhard (1976) and Esbensen (1977). From Fig. 21, it is concluded that the experimental L_1 values are in good agreement with the expression $L_1 = 2L_1^{JM}$. This supports Lindhard's and Esbensen's value for the Z_1^3 correction and thereby the L_1 expression used in the preceding section in connection with the discussion of shell corrections. It should be noted that the deviation of L_1^{exp} from L_1^{JM} cannot be explained as a charge-state effect since the introduction of an effective charge state $Z_{HE}^* < 2$ would increase the L_1^{exp} values in Fig. 21.

Ranges of Σ^+ and Σ^- in emulsion for $v \sim 20v_0$ were found to differ by an amount corresponding to the value given by Lindhard (1976), while the range differences in hydrogen were a factor of five larger than Lindhard's prediction (for a review of the experimental range data, see Heckman (1970)). On this background it is important that the present experimental L_1 for hydrogen agrees with Lindhard's findings. The large uncertainty in $L_1(H_2)$ is due to the high $L(v, Z_2)$ value.

Only Ward et al. (1976) have previously analyzed their data for Z_1^3 effects for $v/v_0 < 5$. They measured stopping cross sections for hydrogen and helium in aluminum and found that, within the experimental uncertainty, the quantity $(S_{He} - 4S_H)/S_{He}$ was equal to zero for $v/v_0 \sim 4.5$. From this they concluded that no Z_1^3 effect was present. However, taking into account the Z_1^4 correction, we find

$$\frac{S_{He} - 4S_H}{S_{He}} = \frac{L_1 + 3L_2}{L + 2L_1 + 4L_2} = 0.84\% \quad \text{for} \quad v/v_0 = 4.5.$$

This is in perfect agreement with the results in Fig. 12 of the paper by Ward et al., and their data hence confirm the magnitude of the higher-order Z_1 effects found in this work.

C. Helium stopping powers.

As mentioned above, it is not possible to make any detailed comparison between S_{He} data and perturbation calculations for a free electron gas at the present energies. In spite of this, Rousseau et al. (1971) have used the Lindhard-Winther expressions for an electron gas with the charge-densities obtained from Hartree-Fock-Slater wave functions to calculate the stopping cross section for 0.4-2 MeV α particles. The calculations, with which Chu and Powers (1971) compare their noble-gas results, are wrong due to problems with the joining of the asymptotic expressions by Lindhard and Winther. Comparing the present S_{He} results with later and corrected calculations by Ziegler and Chu (1974), we find surpris-

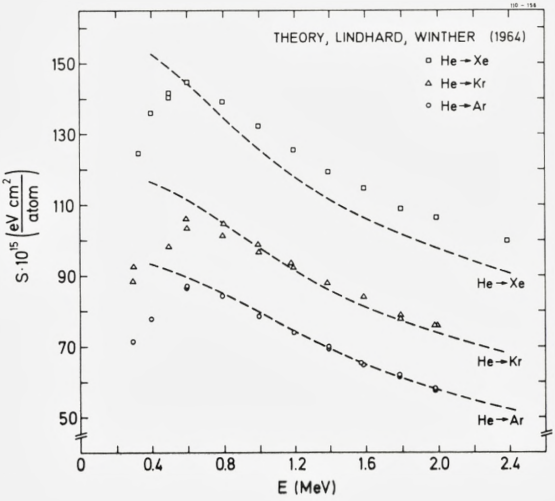

Fig. 22: Stopping cross sections for He penetrating Ar, Kr, and Xe compared with calculations by Ziegler and Chu (1974) based on Lindhard-Winther theory.

ingly good agreement (to within $\pm 7\%$ even at energies as low as $E_{He} \sim 600$ keV). Figure 22 shows the situation for Xe, Kr, and Ar.

D. The ratio S_{He}/S_H as a function of velocity.

As mentioned above, a quantal perturbation calculation of the stopping cross section is restricted to velocities $v > 2v_0 Z_1$. At lower velocities, it has, nevertheless, been suggested that the usual stopping formula (2) be applied with the charge number Z_1 replaced by an effective charge number, i.e.

$$S = \frac{4\pi e^4 Z_2}{mv^2} (Z_1^*)^2 L(v, Z_2) . \tag{30}$$

Many authors have used this approach to analyze experimental stopping-power data in terms of charge states, comparing heavy-ion stopping powers with corresponding proton-stopping powers at the same velocity. It should, however, be emphasized that no theoretical basis exists for this charge-state scaling procedure.

In Fig. 23, the ratio between the present hydrogen and helium stopping powers measured at the same velocity are shown as smooth curves. These data lead to the following conclusions:

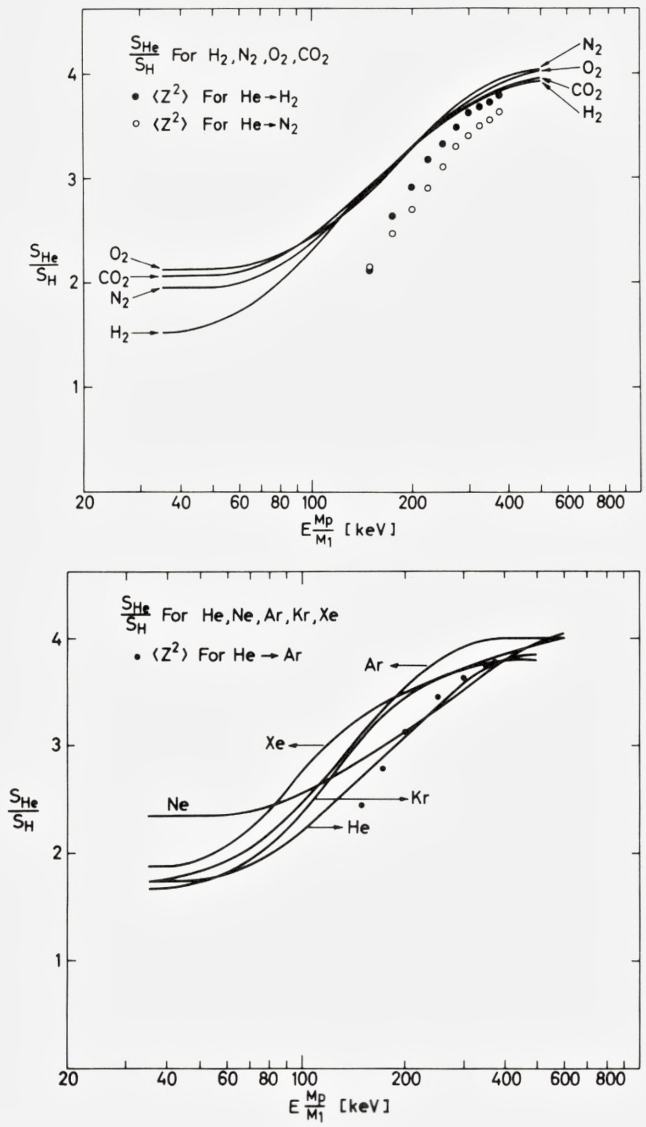

Fig. 23: Experimental stopping-power ratios (solid curves) of He ions to hydrogen ions evaluated at the same velocity, compared with Pivovar's (1961) measured mean-square charge state for He ions in H_2, N_2, and Ar.

(1) The ratios S_{He}/S_H are not independent of Z_2, as was also found by Sautter and Zimmermann (1965). Thus it is not possible, at least not for gases, in a simple way to scale $S_{He}(v, Z_2)$ to $S_H(v, Z_2)$ or vice versa.

(2) From being a constant nearly equal to four for E/amu >500 keV, S_{He}/S_H decreases with decreasing velocity and approaches another constant value for E/amu $\lesssim 50$ keV, and this value depends strongly on Z_2. If the stopping power in the low energy region is written in power form as $S = kE^p$, k and p being constants, the exponents p are approximately equal for hydrogen and helium ions in a given target material. According to the wellknown Lindhard-Scharff (1961) velocity-proportional stopping formula (12), the constant ratio is given by

$$(S_{He}/S_H)^{LS} = 2^{7/6} \frac{(1+Z_2^{2/3})^{3/2}}{(2^{2/3}+Z_2^{2/3})^{3/2}} . \tag{31}$$

In Table III, the experimental ratios are compared with the L-S values for E/amu $\lesssim 50$ keV. Rather good agreement is found for the lighter target elements.

Table III

	H_2	He	N_2	O_2	Ne	Ar	Kr	Xe
exp.	1.53	1.75	1.95	2.15	2.35	1.75	1.65	1.88
L-S	1.53	1.65	1.88	1.90	1.93	2.02	2.09	2.12

It might be noted that our lithium stopping-power results for the same gases (Andersen et al. 1978) at energies 25 keV $\lesssim$ E/amu $\lesssim$ 75 keV, give exponents p which are systematically higher than 0.5 while those for helium are lower than 0.5 (see Table IV in the next section). Thus the S_{Li}/S_{He} ratios are energy-dependent.

(3) From formula (30), the ratio S_{He}/S_H is given by

$$S_{He}/S_H = (Z^*_{He})^2/(Z^*_H)^2 \times L_{He}/L_H . \tag{32}$$

Since $L_{He}/L_H \simeq 1$ and $(Z^*_H)^2 \simeq 1$ for $E_H \gtrsim 150$ keV, one would expect that $S_{He}/S_H \simeq (Z^*_{He})^2$ down to $E(M_p/M) \gtrsim 150$ keV. In Fig. 23, the (S_{He}/S_H) ratios in H_2, N_2, and Ar are compared with the mean-square charge states

$$<Z^2> = \sum_i i^2 \times F_{i\infty} \tag{33}$$

for helium in H_2, N_2, and Ar obtained from equilibrium charge-state measurements by Pivovar et al. (1961). $F_{i\infty}$ denotes the equilibrium charge-state fraction

of the beam in charge state i. A discrepancy of the order of 10% is revealed for E/amu $\lesssim$ 375 keV.

It is concluded that at the one percent level the helium stopping powers, at least for gases, are inconsistent with Eq. (30) with $(Z_1^*)^2$ equal to the mean-square charge state measured directly, and the present results support the theoretical reservation against Eq. (30). The parameter $(Z_1^*)^2$ is no more than a scaling parameter which, on the other hand, appears to be useful for a prediction of unmeasured heavy-ion stopping powers with a required accuracy in the 15 percent range.

Concerning the ratios S_{He}/S_H, it should be emphasized that the S_{He} and S_H results were measured with the same setup. Therefore most of the systematic errors cancel, and this results in rather accurate ratios with $2\sigma \sim 2.8\%$. Many authors have extracted S_{He}/S_H ratios by comparing S_{He} and S_H measured by different groups. In this case, two sets of systematic errors are superimposed.

E. Velocity-proportional region.

For $v < v_0 Z_1^{2/3}$, it has been demonstrated experimentally (see, e.g., Hvelplund and Fastrup (1968) and Hvelplund (1971)) that as a function of Z_1 and Z_2, the electronic stopping exhibits oscillations around the smooth curve given by Eq. (12). These oscillations may be understood in terms of the Lindhard-Scharff picture. The stopping power is proportional to the transport cross section for electrons scattered by a screened LJ potential around the ion, and this cross section exhibits oscillations similar to the one responsible for the Ramsauer-Townsend effect encountered in the scattering of low energy electrons by atoms (Lindhard and Finnemann (1968)). Since the Z oscillations damp out at increasing energies, deviations from the $E^{1/2}$ dependence of S_e are expected, and experimental electronic-stopping cross sections are usually fitted to the convenient form $S_e = k \times E^p$, where k and p are constants. In Table IV, the present S_{He} results for the energy interval of 100-350 keV are presented in this form. (With E expressed in keV, the resulting stopping cross sections are obtained in units of 10^{-15} eV cm^2/atom.)

Table IV

$S_e = kE^p$	H_2	He	N_2	O_2	Ne	Ar	Kr	Xe
k	1.45	1.86	5.46	5.59	3.72	6.85	5.12	7.28
p	0.37	0.36	0.35	0.34	0.39	0.41	0.48	0.49

From Fig. 16, the argon data of Weyl (1953) for $150 \lesssim E_{He} \lesssim 300$ keV are observed to be in perfect agreement with the present results. The energy dependence of the argon and N_2 data of Ormrod (1968) for $10 \lesssim E_{He} \lesssim 100$ keV deviates from that of the present data. It has, however, also been observed in previous experiments that the exponent p may depend rather strongly on the energy interval.

§6. Conclusion

Stopping powers for hydrogen ions in the energy region 40 keV to 1 MeV and helium ions of 100 keV to 2.4 MeV have been measured in H_2, He, N_2, O_2, CO_2, Ne, Ar, Kr, and Xe with an accuracy of $\pm 2.5\%$ (2σ). While the hydrogen-stopping powers show good agreement with most other published data and with Andersen and Ziegler's empirical stopping-power tabulations, the helium-stopping powers are systematically lower than those of the Baylor group by 1-6%. Higher-order Z_1 effects greatly influence the evaluation of shell corrections. With these effects taken into account, the empirical shell corrections, extracted from the experimental proton stopping-power data, are in good agreement with Bonderup's theoretical calculations, based on the Lindhard-Scharff model, at energies as low as $0.1 \lesssim E_H \lesssim 1$ MeV. Experimental I values are extracted and are in satisfactory agreement with those given by Andersen and Ziegler. Z_1^3 correction terms to the Bethe formula have been deduced from the experimental data, and within the accuracy of the experiment, they agree with Lindhard's and Esbensen's value. From a comparison of the stopping powers for helium and hydrogen ions at the same velocity, it has been shown that S_{He}/S_H for $1.25 \lesssim v/v_0 \lesssim 5$ depends strongly on Z_2 and deviates significantly from the mean-square charge states $<Z^2>_{He \to Z_2}$ obtained directly in equilibrium charge-state measurements.

Acknowledgements

We are much indebted to E. Bonderup and J. Lindhard for their continuous interest in the present work and for the help and guidance received from them. The assistance extended to us from the technical staff, especially V. Toft, is gratefully acknowledged. Finally, we wish to thank A. Grandjean and I. Schmidt for their competent assistance in the preparation of the present article.

References

H. H. Andersen, J. F. Bak, H. Knudsen, and B. R. Nielsen, Phys. Rev. *A 16*, 1929 (1977).

H. H. Andersen, F. Besenbacher, and H. Knudsen, Nucl. Instrum. Methods *149*, 121 (1978).

H. H. Andersen, A. F. Garfinkel, C. C. Hanke, and H. Sørensen, Kgl. Dan. Vidensk. Selsk. Mat. Fys. Medd. *35*, No 4 (1966).

H. H. Andersen, H. Simonsen, and H. Sørensen, Nucl. Phys. *A 125*, 171 (1969).

H. H. Andersen and J. F. Ziegler, *Hydrogen Stopping Powers and Ranges in All Elements* (Pergamon, N.Y., 1977).

J. C. Ashley, R. H. Ritchie, and W. Brandt, Phys. Rev. B *5*, 2393 (1972) ibid A *8*, 2402 (1973).

F. Besenbacher, H. H. Andersen, P. Hvelplund, and H. Knudsen (to be published) (1980).

F. Besenbacher, J. Heinemeier, P. Hvelplund, and H. Knudsen, Phys. Lett. *61A*, 75 (1977).

H. A. Bethe, Ann. Phys. *5*, 325 (1930).

H. Bichsel, in: *Studies in Penetration of Charged Particles in Matter*, NAS-NRC Publ. 1133 (1964) p. 17.

F. Bloch, Ann. Phys. *16*, 285 (1933).

F. Bloch, Z. Phys. *81*, 363 (1933).

N. Bohr, Kgl. Danske Vidensk. Selskab, Mat. Fys. Medd. 18, No. 8 (1948).

E. Bonderup, Kgl. Danske Vidensk. Selsk. Mat. Fys. Medd. *35*, No 17 (1967).

E. Bonderup and P. Hvelplund, Phys. Rev. A *4*, 562 (1971).

E. Bonderup and J. Lindhard (1967) (private communication).

P. D. Bourland, W. K. Chu, and D. Powers, Phys. Rev. B *3*, 3625 (1971).

J. E. Brolley and F. L. Ribe, Phys. Rev. *98*, 1112 (1955).

A. B. Chilton, J. N. Cooper, and J. C. Harris, Phys. Rev. *93*, 413 (1954).

W. K. Chu and D. Powers, Phys. Rev. B *4*, 10 (1971).

W. K. Chu and D. Powers, Phys. Lett. *40A*, 23 (1972).

V. Dose and G. Sele, Z. Phys. *A 272*, 237 (1975).

H. Esbensen, Thesis, University of Aarhus (unpublished) (1977).

B. Fastrup, A. Borup, and P. Hvelplund, Can. J. Phys. *46*, 489 (1968).

B. Fastrup, P. Hvelplund, and C. A. Sautter, Kgl. Dan. Vidensk. Selsk. Mat. Fys. Medd. *35*, No 10 (1966).

C. C. Hanke and H. Bichsel, Kgl. Dan. Videnskab. Selsk. Mat.-Fys. Medd. *38*, No 3 (1970).

H. H. Heckman, in: *Penetration of Charged Particles in Matter:* A Symposium: NAS-NRC Publication, Washington, D.C. (1970).

J. Heinemeier, P. Hvelplund, and F. R. Simpson, J. Phys. B *8*, 1880 (1975).

U. Hoyer and H. Wäffler, Z. Naturforsch. *26a*, 592 (1971).

P. Hvelplund, Thesis, University of Aarhus (unpublished) (1968).

P. Hvelplund, Kgl. Dan. Vidensk. Selsk. Mat.-Fys. Medd. *38*, No 4 (1971).

P. Hvelplund and B. Fastrup, Phys. Rev. *165*, 408 (1968).

M. Inokuti, T. Baer, and J. L. Dehmer, Phys. Rev. A *17*, 1229 (1978).

J. D. Jackson and R. L. McCarthy, Phys. Rev. B *6*, 4131 (1972).

G D. Kerr, L. M. Hairr, N. Underwood, and A. W. Walker, Health Phys. *12* 1475 (1966).

H. Knudsen, F. Besenbacher, J. Heinemeier, and P. Hvelplund, Phys. Rev. A *13*, 2095 (1976).

R. A. Langley, Phys. Rev. B *12*, 3575 (1975).

J. Lindhard, Kgl. Dan. Vidensk. Selsk. Mat.-Fys. Medd. *28*, No 8 (1954).

J. Lindhard, in: *Studies in Penetration of Charged Particles in Matter*, NAS-NRC Publ. 1133 (1964) p. 1.

J. Lindhard, Nucl. Instr. Methods *132*, 1 (1976).

J. Lindhard and J. Finnemann, private communication and J. Finnemann, Thesis, University of Aarhus (unpublished) (1968).
J. Lindhard and M. Scharff, Kgl. Dan. Vidensk. Selsk. Mat.-Fys. Medd. *27*, No 15 (1953).
J. Lindhard and M. Scharff, in: *Report on Conference on Penetration of Atomic Particles*. Gatlinburg, 1958, NAS-NRC Publ. 752, (1960) p. 49.
J. Lindhard and M. Scharff, Phys. Rev. *124*, 128 (1961).
J. Lindhard and Aa. Winther, Kgl. Danske Vidensk. Selsk. Mat.-Fys. Medd. *34*, No 4 (1964).
J. H. Ormrod, Can. J. Phys. *46*, 497 (1968).
R. B. J. Palmer, Proc. Phys. Soc. Lond. *87*, 681 (1966).
J. T. Park and E. J. Zimmermann, Phys. Rev. *131*, 1611 (1963).
J. A. Phillips, Phys. Rev. 90, 532 (1953).
L. I. Pivovar, V. W. Tubaev, and M. T. Noikov, Zh. Eksp. Teor. Fiz. *41*, 26 (1961) [Sov. Phys.-JETP *14*, 20 (1962)].
J. J. Ramirez, R. M. Prior, J B. Swint, A. R. Quinton, and R. A. Blue, Phys. Rev. *179*, 310 (1969).
H. K. Reynolds, D. N. F. Dunbar, W. A. Wenzel, and W. Whaling, Phys. Rev. *92*, 742 (1953).
C. C. Rousseau, W. K. Chu, and D. Powers, Phys. Rev. A *4*, 1066 (1971).
E. Rotondi, Radiat. Res. *33*, 1 (1968).
C. A. Sautter and E. J. Zimmermann, Phys. Rev. *A 140*, 490 (1965).
P. Sigmund, Phys. Rev. A *14*, 996 (1976).
E. P. Steinberg, S. B. Kaufman, B. D. Wilkins, C. E. Gross, and M. J. Fluss, Nucl. Instr. Methods *99*, 309 (1972).
J. B. Swint, R. M. Prior, and J. J. Ramirez, Nucl. Instr. Methods *80*, 134 (1970).
J. H. Thorngate, ORNL-TM-5165 (1976).
P. V. Vavilov, Zh. Eksp. Teor. Fiz. *32*, 920 (1957) [Sov. Phys.-JETP *5*, 749 (1957)].
D. Ward, J. S. Foster, H. R. Andrews, I. V. Mitchell, G. C. Ball, W. G. Davies, and G. J. Costa, AECL-5313 (1976).
F. Wenger, R. P. Gardner, and K. Verghese, Health Phys. *25*, 67 (1973).
P. K. Weyl, Phys. Rev. *91*, 289 (1953).
P. K. Weyl and M. T. Burgy (1957) (unpublished); their results are quoted by D. I. Porat and K. Ramavataram, Proc. Phys. Soc. Lond. *A 252*, 394 (1960).
R. L. Wolke, W. N. Bishop, E. Eichler, N. R. Johnson, and G. D. O'Kelley, Phys. Rev. *129*, 2591 (1963).
J. F. Ziegler, *Helium Stopping Powers and Ranges in All Elements* (Pergamon, N.Y., 1978).
J. F. Ziegler and W. K. Chu, Atomic Data and Nuclear Data Tables *13*, 463 (1974).

Indleveret til Selskabet november 1978.
Færdig fra trykkeriet august 1979.

Det Kongelige Danske Videnskabernes Selskab

Matematisk-fysiske Meddelelser

Mat. Fys. Medd. Dan. Vid. Selsk.

Priser excl. moms

Vol. 39 (*uafsluttet/unfinished*)

1. LINDHARD, J.: On the Theory of Measurement and its Consequences in Statistical Dynamics. 1974 ..... 50.–
2. KLEIN, OSKAR: Le principe d'équivalence d'Einstein utilisé pour une alternative de la cosmologie relativiste en regardant le système des galaxies comme limité et non comme l'univers. 1974 ..... 40.–
3. ANDERSEN, NILS, and SIGMUND, PETER: Energy Dissipation by Heavy Ions in Compound Targets. 1974 ..... 50.–
4. SIDENIUS, G.: Systematic Stopping Cross Section Measurement with Low Energy Ions in Gases. 1974 ..... 40.–
5. PEDERSEN, GERT KJÆRGÅRD: Borel Structure in Operator Algebras. 1974 40.–
6. KALCKAR, JØRGEN, and ULFBECK, OLE: On the Problem of Gravitational Radiation. 1974 ..... 40.–
7. MØLLER, C.: A Study in Gravitational Collapse. 1975 ..... 40.–
8. HYNNE, F.: A Class of Molecular Correlation Functions Related to Ursell Functions. 1975 ..... 40.–
9. KALCKAR, JØRGEN, and ULFBECK, OLE: Studies in Classical Electron Theory. I. 1976 ..... 50.–
10. ANDERSEN, J. U.; ANDERSEN, S. KJÆR, and AUGUSTYNIAK, W. M.: Channeling of Electrons and Positrons, Correspondence between Classical and Quantal Descriptions. 1977 ..... 60.–
11. SIGMUND, PETER: Classical Scattering of Charged Particles by Molecules: Single and Multiple Collisions at Small Angles. 1977 ..... 40.–
12. DAHL, JENS PEDER: The Spinning Electron. 1977 ..... 50.–
13. MØLLER, C.: On the Crisis in the Theory of Gravitation and a Possible Solution. 1978 ..... 40.–
14. CRAWFORD, D. L.; OLSEN, E. H., and STRÖMGREN, BENGT: Analysis Based on Determinations of Colour Excesses, Distances, Ages and Masses for Early Group B and A Stars Brighter than $V = 6.^{m}_{5}$ .....

Vol. 40 (*uafsluttet/unfinished*)

1–2. Investigations of Formaldehyde Oxime, its Polymers and Coordination Compounds.

1. Jensen, K. A., and Holm, Arne: On the Nature of the So-Called "Triformoxime" and Isolation of the Authentic Trimer, 1,3,5-Trihydroxyhexahydro–1,3,5-triazine. 1978 ..... 40.–
2. Andersen, Flemming A., and Jensen, K. A.: The Infrared Spectrum of Poly(formaldehyde oxime). 1978 ..... 40.–
3. Besenbacher, F., Andersen, H. H., Hvelplund, P., and Knudsen, H.: Stopping Power of Swift Hydrogen and Helium Ions in Gases. 1979 ... 50.–
4. Rasmusen, Hans Qvade: Three Revolutions of the Comets Halley and Olbers 1759–2024. 1979 ..... 60.–
5. Sigmund, Peter: Statistics of Particle Penetration. 1978 ..... 50.–
6. Aaboe, Asger, and Hamilton, N.T.: Contributions to the Study of Babylonian Lunar Theory. 1979 ..... 50.–

Printed in Denmark by Bianco Lunos Bogtrykkeri A/S. ISSN 0023-3323. ISBN 87-7304-097-5